Influence of multiple elastic and inelastic scattering on photoelectron line shape

Wolfgang S.M. Werner

Institut für Allgemeine Physik, Vienna University of Technology, Wiedner Hauptstrasse 8-10, A 1040 Vienna, Austria

(Received 28 October 1994; revised manuscript received 30 January 1995)

The influence of multiple elastic and inelastic scattering on photoelectron spectra from semi-infinite random solids has been investigated. A theoretical expression describing the energy and angular yield has been derived which adequately accounts for the anisotropic source emission of photoelectrons. Comparison of theory with results from an efficient Monte Carlo code yields very satisfactory agreement. The resulting energy and angular distribution for four subshell transitions in gold are presented. A pronounced dependence of the particle transport on the line shape is seen in the results for different geometries. As an application of the presented theory, a procedure to correct the observable experimental spectrum in the quasielastic regime for multiple elastic and inelastic collisions is developed and tested. In all studied cases the proposed approach yields background corrected spectra agreeing within 3% with the original line shape, while methods not accounting for the anisotropic source emission generally display discrepancies of up to 30% in the background intensity. The main advantage of the proposed approach lies in its generality. It not only accurately describes the influence of particle transport on the energy and angular distribution of Auger electrons and photoelectrons, but can also be applied in a straightforward manner to many other spectroscopic techniques using electrons, ions, or other probing particles.

I. INTRODUCTION

Photoelectron spectroscopy is an important tool for the study of the electronic structure of condensed matter and is moreover a widely used technique for quantitative surface analysis.[1] In line-shape analysis as well as in quantitative peak area evaluation, an accurate theoretical description for the angular and energy distribution is important for the interpretation of experimental data. The spectral features are, to a large extent, determined by the transport of signal electrons between generation in the solid and escape from the surface. Multiple elastic and inelastic collisions significantly modify the particle energy and angular distribution, leading to a distinct difference between the observable experimental spectrum and the true intrinsic spectrum.

Although several empirical methods to extract the necessary information from experimental data have been proposed in the past,[2–6] until recently there has existed no theoretical description accounting for the relevant transport phenomena involved in the photoelectron emission process. In this connection, it seems useful to recall that from the theoretical point of view three regimes for electron transport may be distinguished, governed by the so-called scattering parameter

$$\chi = \lambda_i/\lambda_{\rm tr}. \tag{1}$$

Here λ_i is the electron inelastic mean free path (IMFP) and $\lambda_{\rm tr}$ is the transport mean free path, determining the (large angle) deflection probability. The limit of strong absorption is attained for small values of the scattering parameter ($\chi \ll 1$) when the electron trajectories do not display significant deflections owing to the large probability for energy loss. Therefore, for small scattering parameters, elastic scattering may be neglected and the strong absorption regime coincides with the straight line approximation. In the opposite limiting case of large scattering parameters, on the contrary, electron deflection will dominate the transport process and the trajectories will be diffusionlike. In this case the diffusion or P_1 approximation provides an accurate description of the phenomenon.

Unfortunately, the overwhelming majority of photoelectron transitions is associated with a scattering parameter of the order of unity, $\chi \sim 0.5$, thereby invalidating both the straight line and the diffusion approximation. Recently, the question of how to appropriately address the case of intermediate scattering parameters was resolved by introduction of the so-called generalized radiative field similarity principle.[7–10] This principle states that an accurate approximate solution to the transport equation may be found by replacing the elastic cross section by any approximate cross section subject to three conditions: (1) For small scattering parameters the solutions should reduce to the straight line case; (2) for large scattering parameters the original radiative field similarity should be fulfilled,[11] and (3) the source distribution in the transport equation should be a smooth function of the emission angle. Thus this principle immediately rules out the straight line and diffusion approaches as accurate approximations. The latter is extensively used, however, and easy to use background subtraction procedures have been derived in the framework of this approximation.[12–17] On the other hand, the generalized radiative field similarity principle fully substantiates the so-called transport approximation with the essential provision that the source angular distribution should be sufficiently smooth. Several authors have used the transport

approximation to study various problems connected with medium energy electron transport.[7,10,16,18,19] Recently a simple and effective description of isotropic Auger emission was developed in the framework of the transport approximation in Ref. 7. Comparison with Monte Carlo (MC) model calculations demonstrated the high accuracy of this method and in particular substantiated the emission angle dependence of the shape of the energy distribution this theory predicts, a previously unknown effect.

None of the aforementioned approaches accounts for the fact that the source distribution in the photoelectron emission process is anisotropic in general. Meanwhile, extensive investigations concerning the influence of electron transport on the angular distribution of photoelectrons revealed that elastic scattering significantly modifies the emitted angular distribution.[9,20–22] Since the shape of the energy spectrum is closely connected with the angular distribution of the emission process, it seems worthwhile to study the influence of anisotropic source emission on the photoelectron line shape.

In the present paper, the influence of multiple elastic and inelastic scattering on the yield for anisotropic photoelectron emission is investigated. On the basis of the generalized radiative field similarity principle, the transport approximation is applied to derive a theoretical expression for the emission characteristics, i.e., the energy and angular yield of a homogeneous random sample. The so-called (integrated) partial escape distributions (PED's) play a central role in this theory. These quantities are defined as "the probability that an electron generated at an arbitrary depth in a homogeneous sample is emitted from the surface with its direction in a certain angular interval after experiencing a given number of inelastic collisions." It should be emphasized that an expression for the partial escape distributions (or the partial reflection distributions in a reflection geometry) is the key step in solving the transport problem for many spectroscopic techniques in the quasielastic regime, i.e., when the scattering characteristics depend only insignificantly on the energy of the particle.

The partial escape distributions calculated in the transport approximation are compared with results of an efficient numerical MC model, employing the reciprocity theorem for one-speed transport.[23] Satisfactory agreement is found between the two approaches, the agreement being better for smoother initial angular distributions, thereby fully corroborating the generalized radiative field similarity principle.

Quite pronounced effects of the anisotropic source emission are observed in the energy spectra, not accounted for by previous theories. A background subtraction method is proposed which accounts for these effects. It is conceptually simple, numerically stable, and exhibits good convergence behavior. Application of this method to model spectra yields almost perfect background removal. The most important advantage of this method is, however, that it is applicable to problems with arbitrary dependences of the partial escape distributions on the geometry and the number of inelastic collisions. In view of the fact that the spectral features of many a spectroscopic technique may be described in terms of partial escape distributions in a fashion fully analogous to the presented approach, this implies that the proposed method is of quite general validity and may also be useful in areas of physics other than photoelectron spectroscopy.

II. THE MONTE CARLO METHOD

The Monte Carlo technique is used in the present work exclusively to calculate the (geometry dependent) partial escape distributions. The basic model assumptions are described in detail elsewhere[24] and agree with the commonly accepted model for the transport of medium energy electrons in random solids. In principle all that is needed are randomly generated values for the scattering angles and the step lengths between elastic collisions. The former are generated from the Mott cross section for elastic scattering while the latter are drawn from the distribution of elastic path lengths which is assumed to obey Poisson statistics with the elastic mean free path as characteristic length.

The important difference between the present model and the conventional techniques is the application of the reciprocity theorem,[23] which has been successfully employed previously in similar studies.[25,18,26] This theorem is an expression of a symmetry property of the Boltzmann equation and applies to the quasielastic case. It states that, if the detector and the source in a given transport problem are interchanged, the corresponding particle flux density can be obtained from the original one by simply changing the sign of directional variables. In a MC model calculation this means that an electron trajectory is generated in reverse, i.e., it starts outside the solid, with a direction corresponding to the analyzer geometry, and is subsequently traced back.

In the present implementation, the contribution of a trajectory to the partial escape distribution P_n is assumed to increase with the path traveled in the solid. From this it follows immediately that the scattering process is governed by Poisson statistics.[24] Since we are only interested in the partial escape distributions integrated over all depths the contribution of a segment of a trajectory between the lth and $(l+1)$st elastic collision may be written as

$$\Delta P_{n,l} = q(\vec{\Omega}_l) \int_{\Lambda_l}^{\Lambda_l + \Delta\Lambda/|\mu_l|} \mathcal{P}_n(z)dz, \tag{2}$$

where $\mathcal{P}_n(z)$ is the Poisson distribution:

$$\mathcal{P}_n(z) = \frac{1}{n!}(z/\lambda_i)^n \exp(-z/\lambda_i).$$

Further, Λ_l is the path length traveled just before the lth elastic collision, $\Delta\Lambda$ is the steplength between the lth and $(l+1)$st scattering, and $\mu_l = \arccos(\psi_l)$ is the polar direction of the electron on this part of the trajectory, measured along the surface normal. To account for the anisotropic source emission distribution, the contribution is weighted with the source angular distribution $q(\vec{\Omega}_l)$ in

the actual direction of the particle $\vec{\Omega}_l$. After partial integration of the above equation and some transformations, the following recursion formula can be derived allowing for an efficient calculation of the contributions to the signal:

$$\frac{\Delta P_{n,l}}{q(\vec{\Omega}_l)} = -\lambda_i\{\mathcal{P}_n(\Lambda_l + \Delta\Lambda/|\mu_l|) - \mathcal{P}_n(\Lambda_l)\} + \Delta P_{n-1,l},$$

$$\Delta P_{-1,l} = 0.$$

After calculating a certain number of trajectories, the P_n probabilities are obtained in units of sterad^{-1} s^{-1} Å^{-2} by dividing the total intensity through the number of trajectories, assuming that the number of electrons generated per second in a unit volume equals unity.

A final remark regarding the termination criterion is in place at this stage. Those trajectories which leave the solid after some elastic processes are taken to contribute to the signal but only their path length traveled within the solid is used. As soon as the electron leaves the solid, its trajectory is terminated. If it remains inside the solid, it is terminated after its pathlength exceeds $10N\lambda_i$ where N is the highest order of inelastic scattering of interest.

The advantage of the adopted approach should be sufficiently clear: the required computing time is reduced by quite a few orders of magnitude for a given statistical accuracy. To see this, note that in the conventional scheme many trajectories are generated which do not lead to emission at all. If emission does take place, it is still questionable whether the emission direction corresponds to the analyzer geometry and again a considerable amount of trajectories is generated in vain. An assessment shows that for isotropic source emission, where advantage may be taken of the azimuthal symmetry, calculation of the partial escape distribution of zeroth order (i.e., those electrons which are not inelastically scattered at all and contribute to the peak intensity) requires $\sim$ 10 h. In a situation without azimuthal symmetry for an opening angle of the detector of, let us say, 1°, the computation time is of the order of a month. If higher order PED's are also required the computation time will be around a year, for one given angular distribution and geometry. With the present algorithm, on the same machine (an α-AXP PC), the same statistical significance of the results is achieved in $\sim$1 s per datum, with infinite angular resolution for an arbitrary geometry.

III. THEORY

The starting point of our considerations is a Boltzmann type transport equation.[7,18] Comparison of experimental results with model calculations and analytical results supports the considerations of Ref. 27 from which it follows that such an approach is also justified for polycrystalline materials. However, a slight modification of the scattering characteristics may be necessary in this case.[28] In what follows this may be accounted for by the use of an appropriate value of the transport mean free path in the solution of the transport problem.

The yield of electrons emitted from a semi-infinite solid sample comprises the contributions from particles having experienced a different number n of inelastic collisions. The energy distribution of these contributions is given by the partial loss distributions, being determined by the single scattering loss probability or differential inverse inelastic mean free path (DIIMFP). On the other hand, the amount of electrons belonging to a specific group of n-fold inelastically scattered electrons is just given by the partial escape distributions. The latter quantities are a function of the IMFP and contain all information about the elastic scattering process. Multiplying the loss distribution with the associated escape probability, the partial contribution to the yield is obtained. Clearly, the energy and angular distribution is a superposition of these contributions. Note that this approach presupposes that the influence of energy loss and deflection may be separated. In the present case this is allowed since it is assumed that in the quasielastic regime the characteristic path lengths for loss and deflection vary only slightly in the considered energy range. Moreover, deflections in inelastic collisions may be neglected since the characteristic length for large angle deflections in the course of inelastic processes exceeds the corresponding quantity for elastic scattering by at least two orders of magnitude in general.

With the above considerations in mind, it is easy to see that the general expression for the combined energy and angular distribution $Y(E,\vec{\Omega})$ for a homogeneous sample reads[7]

$$Y(\vec{\Omega},E) = A\lambda_{\rm tr}\sum_{n=0}^{\infty}\int_0^{\infty} dE' f(E')L_n(E-E')P_n(\vec{\Omega}), \tag{3}$$

where A is the electron generation rate and f is the true intrinsic spectrum. The direction of the emitted particles $\vec{\Omega}$ is specified by the polar emission angle $\psi = \arccos\mu$ (defined relative to the outward surface normal) and the azimuthal angle ϕ. To account for the change in the surface area seen by the analyzer at different emission angles in a typical x-ray photoelectron spectroscopy (XPS) geometry, Eq. (3) differs by a factor μ from the result in Ref. 7. The partial loss distributions L_n represent the probability distribution for an energy loss in a certain interval (E, dE) after n inelastic collisions. These quantities are given by an n-fold self convolution of the (normalized) differential inverse inelastic mean free path $w(T)$ as a function of the energy loss T:

$$L_0(T) = \delta(T),$$

$$L_n(T) = \int_0^T dT_0 L_{n-1}(T_0)w(T-T_0). \tag{4}$$

Note that we have anticipated the use of the transport approximation by writing the transport mean free path in the prefactor of Eq. (3). This quantity is defined by

$$1/\lambda_{\rm tr} = N_a\int_{-1}^{1}\frac{d\sigma_e}{d\mu_s}(\mu_s)(1-\mu_s)d\mu_s,$$

where N_a is the atomic density of the material and $d\sigma_e/d\mu_s$ is the elastic cross section, differential with re-

spect to the cosine of the scattering angle μ_s. In the exact solution of the transport equation the elastic mean free path λ_e should be substituted in Eq. (3).

Furthermore, the PED of higher order may be calculated from the zero order result by differentiation with respect to the single scattering albedo:[7]

$$P_n(\vec{\Omega}) = \frac{1}{n!}\left[\frac{\partial^n}{\partial p^n} P_0(\vec{\Omega}, \omega(p))\right]\Bigg|_{p=0}, \tag{5}$$

where $\omega(p)$ is the complex single scattering albedo which in the transport approximation reads

$$\omega(p) = \left[1 + \frac{\lambda_{\rm tr}}{\lambda_i}(1-p)\right]^{-1}.$$

Again, the usual albedo is obtained by replacing $\lambda_{\rm tr}$ by λ_e in this expression. An expression for the zero order PED in the case of an azimuthally symmetric situation has been derived earlier in the transport approximation.[9] It is

$$P_0(\mu) = \frac{\omega^2 H(\mu,\omega)}{2\sqrt{1-\omega}} - \int_0^1 \frac{\mu_0 \omega^2}{2(\mu+\mu_0)} H(\mu,\omega) H(\mu_0,\omega)\bar{q}(\mu_0)d\mu_0 + \omega\bar{q}(\mu). \tag{6}$$

The function $H(\mu,\omega)$ is the Chandrasekhar H function for an isotropically scattering medium[29] and $\bar{q}(\mu)$ is the azimuthally averaged source angular distribution.

The first term in Eq. (6) represents that part of the particle flux density which, on escape from the surface, is sufficiently randomized and consequently this term is independent of the source angular variable. The third term obviously accounts for the contribution of those electrons which do not participate in (large angle) elastic processes at all, while the second term corresponds to those electrons which are scattered but not yet fully randomized.[9]

The corresponding escape probability $P_0(\vec{\Omega})$ for a problem without azimuthal symmetry is obtained by dividing the first two terms of Eq. (6) by 2π, while in the third term $\bar{q}(\mu)$ should be replaced by $q(\vec{\Omega})$. This generalization follows from the linearity of the transport equation and is intuitively clear from symmetry considerations. The remaining problem to describe the general photoelectron angular and/or energy yield is to perform the differentiation in Eq. (5) using the expression for the zero order PED given by Eq. (6). This leads to (see the Appendix)

$$P_n(\vec{\Omega}) = \frac{I_1(\mu)}{4\pi} - \frac{1}{4\pi}\int_0^1 \frac{\mu_0 I_2(\mu,\mu_0)}{(\mu+\mu_0)}\bar{q}(\mu_0)d\mu_0 + q(\vec{\Omega})\frac{\chi}{(\chi+1)^n}. \tag{7}$$

Expressions for the quantities I_1 and I_2 are given in the Appendix.

IV. SEPARATION OF EXTRINSIC AND INTRINSIC PARTS OF THE PHOTOELECTRON SPECTRUM

As one of the main applications of the presented theory we will consider the problem of separation of the extrinsic and intrinsic features of a given spectrum, i.e., the extraction of the true intrinsic spectrum from the observable spectrum containing features due to the particle transport. The usual procedure in finding a deconvolution scheme for distributions of the type Eq. (3) is to perform a Laplace transform on the energy variable, which is trivial observing the convolution theorem. The next step consists in making use of some kind of recursion property of the quantities P_n in such a way that the inverse transform poses no major difficulties, eventually yielding the true intrinsic spectrum f. As is shown in the next section, the dependence of P_n on the number of inelastic processes n may be quite complex in general and it would thus be desirable to develop a deconvolution scheme for an arbitrary series of P_n. It will be shown that this can be achieved in a quite simple way.

We start with the usual step of performing the Laplace transform of Eq. (3) on the energy E. Dropping the variables for clarity and denoting the quantities in Laplace space with a tilde $\tilde{}$ we may write

$$\frac{\tilde{Y}}{A\lambda_{\rm tr}} = \sum_{n=0}^{\infty} \tilde{w}^n \tilde{f} P_n. \tag{8}$$

Introducing the reduced quantities $y = Y/P_0 A\lambda_{\rm tr}$, $p_n = P_n/P_0$, and rearranging we find

$$\frac{\tilde{y}}{\tilde{f}} = 1 + \sum_{n=1}^{\infty} p_n \tilde{w}^n. \tag{9}$$

Now we multiply Eq. (9) by $(1-p_1\tilde{w})$, effectively increasing the exponent on the right-hand side by 1:

$$(1-p_1\tilde{w})\frac{\tilde{y}}{\tilde{f}} = 1 + \sum_{n=2}^{\infty}(p_n - p_1 p_{n-1})\tilde{w}^n, \tag{10}$$

and note at this point that for isotropic source emission we have $p_n = \kappa^n$.[7] Consequently the sum in Eq. (10) vanishes. Therefore, by going back to energy space, we immediately find the deconvolution formula by Tilinin and Werner,[7] derived in a slightly different fashion and valid for an isotropic source distribution:

$$f(E) = y(\mu,E) - \kappa(\mu)\int_E^{\infty} dE' y(\mu,E') w(E'-E). \tag{11}$$

The present derivation of this deconvolution scheme is instructive in that it provides a clue as to how to proceed in the case of an arbitrary series of PED's: we have to select the terms of leading powers of $\tilde{w}$ in the sum on the right-hand side of Eq. (10) and multiply the entire equation by the corresponding term minus unity. In this way, the exponent of the leading term in the sum is increased by 1. Note that in energy space this means that only increasingly larger energy losses contribute to the loss features in the spectrum, while for low losses their inten-

TABLE I. The first six coefficients in the general deconvolution procedure Eq. (13).

a_1	=	p_1
a_2	=	$p_2 - a_1^2$
a_3	=	$p_3 - a_1a_2 - a_1^3$
a_4	=	$p_4 - a_1a_3 - a_2^2 - a_1^2a_2 - a_1^4$
a_5	=	$p_5 - a_4a_1 - a_2^2a_1 - a_1^2a_3 - a_2a_1^3 - a_2a_3 - a_1^5$
a_6	=	$p_6 - a_5a_1 - a_1^2a_4 - a_1^2a_2^2 - a_1^3a_3 - a_1^4a_2 - a_1a_2a_3 - a_2a_4 - a_2^3 - a_1^6$

sity vanishes. Thus the spectrum is consecutively wiped clean, so to speak. On the other hand the left-hand side will be given by a multiple convolution (in energy space) which is still readily evaluated numerically.

Proceeding in this way we find

$$\prod_{n=1}^{N}(1 - a_n\widetilde{w}^n)\widetilde{y} = \widetilde{f} + O(\widetilde{w}^{N+1}). \tag{12}$$

Neglecting terms of order $O(\widetilde{w}^{N+1})$ and going back to energy space, we finally find the general deconvolution scheme

$$f(E) = W_\mu^N[y(E,\mu)], \tag{13}$$

where the operator W_μ^n is defined recursively as

$$W_\mu^n(y) = W_\mu^{n-1}(y) - a_n(\mu)\int_E^\infty L_n(E'-E)W_\mu^{n-1}(y)dE' \tag{14}$$

and $W_\mu^0(y) = y(E,\mu)$. The coefficients a_n are found to be given by

$$a_n = p_n - S_n, \tag{15}$$

where S_n is a sum which defies formal notation while following a simple rule: it contains terms of all possible products of all possible powers of $a_{j<n}$ such that the subscripts in a term taken to the corresponding power add up to n. For convenience, the first few coefficients are shown in Table I, from which it is very easy to grasp the general rule for the generation of the coefficients. Note that for isotropic source emission, when $p_n = \kappa^n$, all coefficients except a_1 vanish and Eq. (13) reduces to the result for isotropic emission Eq. (11).

It should be emphasized again that the deconvolution scheme contained in Eqs. (13)–(15) is generally applicable to problems of the type Eq. (8). In particular this means that by using appropriate PED's removal of multiple scattering features in ion scattering spectroscopy, elastic peak electron spectroscopy, etc., is straightforward. This seems to be the main advantage of the proposed approach.

V. RESULTS AND DISCUSSION

For the comparison of theory with MC calculations and a first test of the deconvolution method, we limit the presentation of the results to the $4s$, $4p$, $4d$, and $4f$ subshells of gold, excited by Mg $K\alpha$ radiation. Results obtained for Al and Cu are qualitatively similar to the presented data, demonstrating that the influence of elastic scattering is not determined by the magnitude of the cross section alone. True, the cross section (and in particular its backward part) decreases with the atomic number and increasing energy, but the point is that the inelastic scattering properties display a very similar dependence, as quantum mechanical considerations show.[30] Consequently, the most important parameter governing the influence of elastic scattering, the scattering parameter, is only very weakly dependent on the energy and atomic number. Therefore, to keep the presentation clear, the results for the other elements may be omitted without loss of generality.

In Table II the main parameters for the analysis are presented for the $4s$, $4p$, $4d$, and $4f$ transitions in Au. The inelastic mean free paths were taken from Ref. 31. The differential inelastic mean free path used in the MC model were calculated from optical data, compiled in Ref. 32, using Penn's algorithm.[33] The transport mean free path was calculated from its definition using the relativistic Mott cross section calculated with the partial wave expansion method[34] employing a Thomas-Fermi-Dirac potential specified by the parameters given in Ref. 35. The cross section calculated in this way was also used in the MC calculations. Note that the scattering parameter χ for the considered transitions is very close to 0.5 for all different subshells in spite of the fact that the considered kinetic energies range from ~500 to 1200 eV, and the transport and inelastic mean free paths display a significant energy dependence. For the source angular distribution the usual differential photoelectron cross section was used:[36]

$$q(\vec{\Omega}_0, \vec{\Omega_\gamma}) = \frac{1}{4\pi}\left[1 - \frac{\beta_x}{4}(3\mu_r^2 - 1)\right], \tag{16}$$

where $\vec{\Omega}_\gamma$ is the direction of the incident photons and μ_r is the cosine of the angle between the direction of incidence of the photons and emission of the signal electrons. Integrating Eq. (16) over the azimuthal angle, the quantity $\bar{q}(\mu)$ is obtained:

TABLE II. Main parameters characterizing the Mg $K\alpha$ excited photoelectron transitions in Au as used in the present work.

Transition	E_k (eV)	λ_i(Å)	λ_{tr}(Å)	χ	β_x
Au $4s$	491	8.5	15.9	0.55	1.82
Au $4p$	707	10.8	18.3	0.59	1.25
Au $4d$	918	13.0	21.7	0.60	1.12
Au $4f$	1169	15.4	26.6	0.58	1.01

$$\bar{q}(\mu,\mu_\gamma)=\frac{1}{2}\left[1-\frac{\beta_x}{8}(3\mu_\gamma^2-1)(3\mu^2-1)\right].$$

The total photoelectron cross section $\sigma_{\rm ph}$ and photoelectron generation rate A were taken to be unity for convenience since we are not interested in relative peak areas in the present work. The asymmetry parameter β_x was taken from Ref. 37.

A survey of the photoelectron angular distribution for two experimental configurations is shown in Fig. 1. The first setup, shown in the inset of Fig. 1(a), is a transmission geometry for a fixed incidence angle of the x rays and a variable emission angle. The data points represent the results of MC calculations while the solid lines represent the theoretical result Eq. (6). For comparison, the results of the straight line approximation are also shown as dotted lines. The roman numerals indicate the geometries used in the further analysis. Although the setup in Fig. 1(a) is convenient for a fundamental study of the influence of elastic scattering,[20,21,38] it suffers from some drawbacks for quantitative analysis. First of all, the intensity at normal emission is rather low and, moreover, the influence of elastic scattering is the most pronounced in this case, as can be clearly seen in Fig. 1. This severely complicates quantification. Therefore the so-called magic angle geometry is usually preferred on commercial spectrometers. This corresponds to a geometry where the differential photoelectron cross section is independent of the parameter β. Such a geometry is approximately attained at normal emission when the angle of incidence of the x rays amounts to 60° (off normal), as indicated by geometry IV in Fig. 1(b).

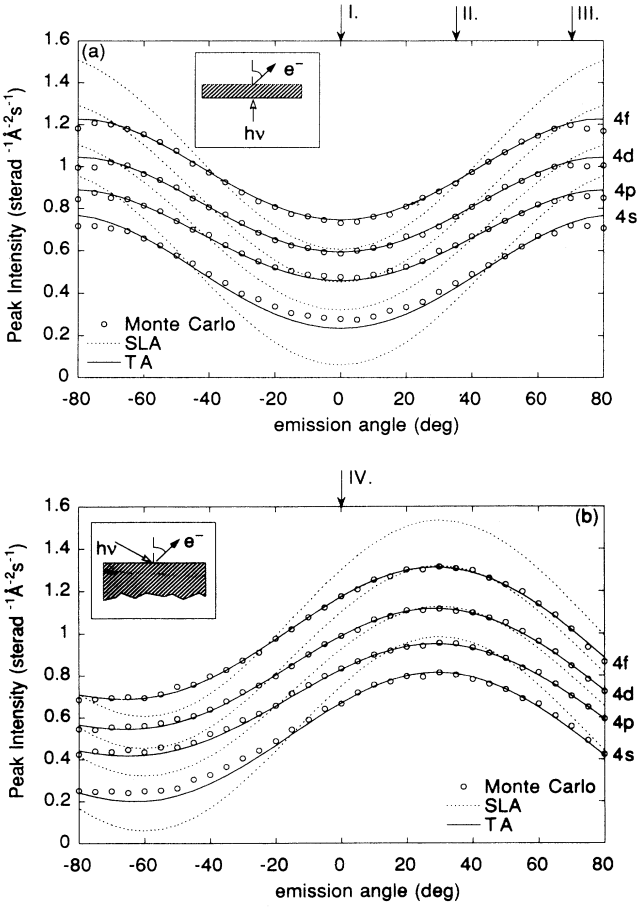

FIG. 1. Angular distribution of the photoelectron transitions investigated in the present work for the geometries indicated in the insets. The data points are the results of MC calculations, the solid lines represent the analytical calculations, as per Eq. (3) and Eq. (7). The straight line approximation is also shown as dotted lines for comparison.

The results in Fig. 1 display a few quite interesting features. First of all, one can observe that in neither configuration does the magic angle geometry coincide with the geometry for which the straight line approximation and MC results intersect. This means that even in the magic angle geometry the influence of the anisotropic source emission on quantification cannot be disregarded. This phenomenon has been extensively discussed by Jablonski and Powell[22] who introduced the so-called master angle to overcome this difficulty.

Furthermore, it may be noted that the overall agreement between theory and the Monte Carlo results is excellent for the outer subshell transitions with low values of the asymmetry parameter, while discrepancies of at the most 15% are seen for the $4s$ transition at normal emission. According to the generalized radiative field similarity principle, this may be attributed to the fact that the source angular distribution is less smooth in the latter case (cf. the straight line approximation results in Fig. 1).

At larger emission angles ($\gtrsim 70°$) systematic discrepancies between the two approaches are seen, in particular in Fig. 1(a). These discrepancies can be entirely explained by the fact that at larger emission angles the transport approximation has an essential deficiency. To fully appreciate this, it is useful to recall the reciprocity theorem which was used as a basis for the present calculations. Two kinds of trajectories contribute to the yield in the reverse trajectory picture: the first have their point of origin within the solid, while the second class are reflected near the surface and are truncated at the solid-vacuum interface. Clearly, the latter class will on the average travel a shorter distance in the solid and consequently contribute less to the yield as per Eq. (2). Therefore, for those geometries where the reflection probability is high, the yield will consequently be low. In the reverse trajectory picture, emission angles $\gtrsim 70°$ correspond to the forward scattering peak present in every elastic cross section, irrespective of the atomic number and energy. This means that for such a geometry the reflection probability is relatively high and, what is even more important, it varies appreciably in a small angular interval around the considered geometry. It is quite clear that the transport approximation, being based on an isotropic cross section, is essentially unable to account for the latter effect.

Some examples for the key quantities concerning the influence of the source anisotropy on the observable line shape, the partial escape distributions, are presented in Fig. 2 for geometries I, II, and III for the Au $4s$ and Au

$4f$ angular distributions. As anticipated in the previous section, these quantities display rather complex characteristics for anisotropic source emission. For geometry III, a monotonic decrease with n is seen for both subshells. The PED for geometry II for the Au $4s$ transition depends only very weakly on the number of inelastic collisions while a monotonic decrease is again seen for Au $4f$. For geometry I, in both cases a maximum in the PED is observed which is attained around $n = 4$ for Au $4s$, while for Au $4f$ it is located around $n = 2$. The agreement between the MC and analytical results [calculated with Eq. (7)] is again better for the smoother source distribution, as the generalized radiative field similarity principle predicts.

The complex dependence of the PED on n has a clear physical explanation: for those emission geometries at which the source angular distribution is low, or even vanishes in some cases, a particle has to be deflected several times before it can be emitted in the regarded direction, whereas the probability that many particles are emitted in this direction without any scattering at all is very small. Thus it requires a certain amount of isotropization of the particle flux density in order to provide substantial intensity in those directions, while in geometries with high source intensities in the regarded direction (e.g., geometry III), a considerable amount of particles can reach the analyzer without any deflection. The isotropization required for escape, e.g., in geometry I, implies enhanced path lengths in the solid between generation and escape. Consequently, the value of the higher order PED's may exceed the elastic escape probability. On the other hand, in geometry III, on the basis of the same considerations, the path length distribution is expected to decrease monotonically with depth and consequently the PED will also decrease with the number of inelastic collisions.

Inserting the values for the PED's thus obtained into Eq. (3), weighting the corresponding partial loss distribution with these quantities, and adding the relevant terms, the energy distribution is obtained. An example of this procedure is shown in Fig. 3 for geometries I and III for the Au $4s$ line. Here and below, a Lorentzian of unity peak area and 1.0 eV full width at half maximum (FWHM) is used as the model true spectrum for simplicity. The (weighted) partial loss distributions associated with 0–7 inelastic collisions are presented in this figure as dotted lines. It is of practical importance to note that the first 100 eV of the loss features in the spectrum are

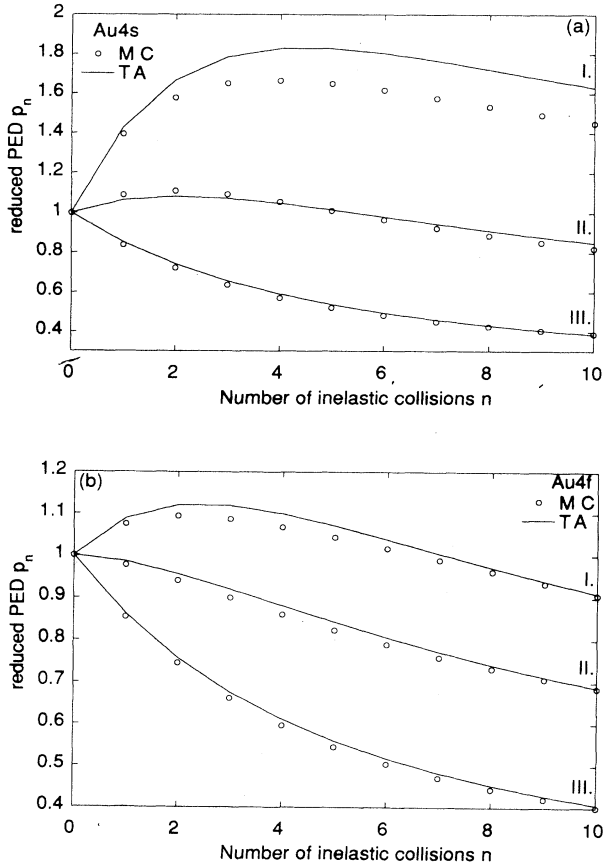

FIG. 2. Reduced partial escape distributions calculated with the MC technique and the expression for the PED given in the Appendix [Eq. (A8)] for the Au $4f$ and Au $4s$ transition and for the indicated geometries.

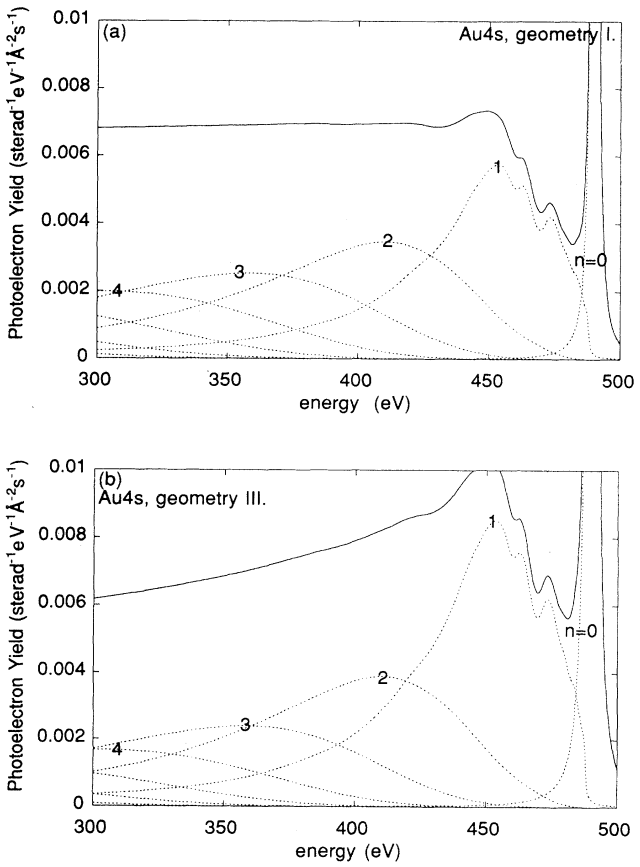

FIG. 3. Total energy spectrum for Au $4s$ for geometries I and III. The contributions of electrons having experienced a given number of inelastic collisions n are also shown as dotted lines.

almost entirely determined by the PED's of order ≤ 3. In the quasielastic regime the upper kinetic energy to which a particular loss distribution of order n contributes is generally seen to be $\sim n\langle w(T)\rangle$ where $\langle w(T)\rangle$ denotes the mean energy loss in a collision, which is usually of the order of the binding energy of outer shell electrons $\sim e^2/a_0 \approx 28$ eV. It is also seen that for $n > 1$ the structure present in the DIIMFP has entirely disappeared. This is of course due to the fact that for Au the loss function in itself is a rather smooth function of the loss energy. For a nearly free electron material (like Al) with a strong plasmon feature in the loss function, a different behavior is observed in this respect.

The different weighting of the loss distributions with the geometry dependent escape distributions is seen to markedly affect the total spectrum, drawn as a solid line. Whereas the background is almost completely flat for geometry I, the low loss features are strongly emphasized at oblique emission (geometry III), and a monotonic decrease is seen at larger loss energies. The maximum in the loss features differs by almost a factor of 1.4 in these two geometries. This difference is entirely due to the different behavior of the partial escape probabilities for these geometries [see Fig. 2(a)]. While the peak areas for these two geometries, or what is equivalent, the zero order escape probability, differ by a factor of 2 [cf. Fig. 1(a)], the yield at larger loss energies $\gtrsim 100$ eV, corresponding to $\sim$5 inelastic collisions, varies only very slowly with the emission angle. This means that the flux isotropization responsible for the behavior of the partial escape distributions is directly observable in the angular distribution of the yield, in particular at larger loss energies.

In Figs. 4(a)–6(a) a survey of the energy distributions of the main photoelectron lines in Au is presented as solid lines for the geometries indicated in Fig. 1. The effect of increasing isotropization of the angular intensity with energy loss is also seen in the case of the Au $4f$ line, although the intrinsic angular distribution is already much smoother than for the $4s$ transition. Since the asymmetry parameters of the $4s$ and $4f$ lines are representative for the highest and lowest anisotropy generally encountered in the photoelectron emission process, it may be concluded that the influence of the source emission angular distribution discussed above is generally observable in the photoelectron line shape.

A comparison of the energy spectra of all four subshell transitions for the magic angle geometry is shown in Fig. 6(a). The background intensity is seen to increase directly proportionally to λ_{tr} (cf. Table I). However, the peak intensities (presented in Fig. 1) exhibit the same increase so that the relative contribution of peak and background to the spectrum is the same in all cases. In other words, the influence of multiple elastic and inelastic scattering is quantitatively similar. The reason is that the partial escape distributions only depend on the scattering parameter χ as per Eqs. (A5)–(A8) while the total yield is proportional to λ_{tr} [see Eq. (4)]. Since the scattering parameter varies only very slowly with energy and atomic number, the relative contributions of intrinsic and extrinsic effects in photoelectron spectroscopy are always of the same order of magnitude. This is in perfect accordance with the result of many experimental studies (see Ref. 13 and references therein).

So far, the Monte Carlo results for the partial escape distributions have been compared with analytical calculations and the resulting effect of the source anisotropy has been investigated. A very satisfactory agreement between the two approaches has been found and where discrepancies occur they are readily understood on a simple physical basis.

The rest of this section will be devoted to separation of intrinsic and extrinsic features in an experimental spectrum. The results obtained by applying Eqs. (12)–(14) will be compared with the widely used background subtraction procedure due to Tougaard and Sigmund,[12] which was later modified by Tofterup[15,17] to account for

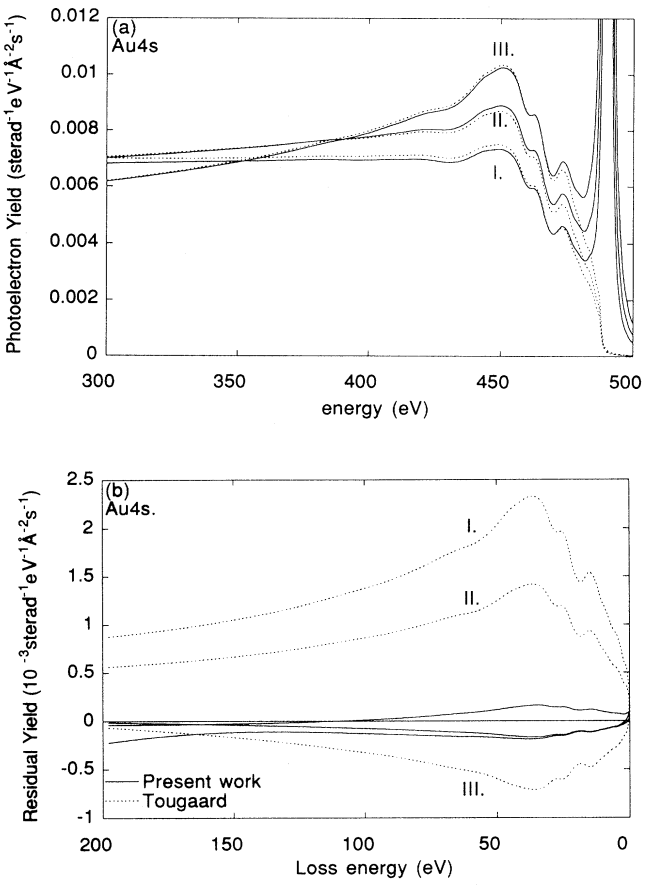

FIG. 4. (a) Au $4s$ subshell transition spectra in the vicinity of the peak for the three geometries indicated in Fig. 1(a). Solid lines: model spectra calculated with the Monte Carlo model and Eq. (3). Dotted lines: contribution of the inelastic background to the spectrum according to Eq. (13). (b) Residual yield after background subtraction. The residual yield is given by the difference between the true intrinsic spectrum and the spectrum obtained by applying the background subtraction Eq. (13) to the model spectra in (a). Solid lines: present work Eq. (13). Dotted lines: result of the Tougaard algorithm. Note that the ordinate scale differs by a factor of 1000 from (a).

elastic scattering in an approximate way. Although it was derived on the basis of isotropic source emission, it is also extensively applied in XPS and its accuracy is generally claimed to be very high.[39] This method may be regarded as a first order approximation to result Eq. (11) in that it does not account for an emission angle dependence of the energy spectrum, which even exists for isotropic source emission.[7] It is obtained by replacing $\kappa(\mu)$ by $L/(L+\lambda_i)$ in Eq. (11), where L is a characteristic length of the path length distribution which, in the framework of the P_1 approximation, is found to be close to $5\lambda_{\rm tr}$.[15] The DIIMFP's usually employed in this method is the universal cross section of Tougaard.[39] In order to meaningfully analyze the present data with Tougaard's method and compare it with the proposed approach, the same DIIMFP's as used in the MC model calculations were used in both background subtraction methods.

For the present method, the maximum number N of deconvolution passes was determined by monitoring the change of the total spectral area after successive passes. The considered energy interval was taken to be 200 eV, which strictly speaking already exceeds the true quasielastic regime in most cases. The deconvolution was terminated after the relative change in the peak area dropped below some small number ϵ. Generally, ϵ will be determined by the measurement statistics. Due to the particular way in which our data were generated, the choice of ϵ (below a certain small value of course) almost did not affect termination, which was in all cases achieved after 6–8 passes. It is believed that this will not change for realistic (noisy) data since higher passes do not affect low loss energies [cf. Fig. 3 and Eq. (13)]. This is a very convenient feature of this method, since it allows one to estimate the required number of passes in advance according to the rule of thumb

$$N \approx \Delta T/\langle w(T)\rangle,$$

where ΔT is the considered energy (loss) interval and $\langle w(T)\rangle$ is the mean energy loss in an inelastic collision. The earlier background subtraction methods are, so to speak, single pass versions of the present one, but only valid for isotropic source emission [cf. Eq. (11)]. In the general case of anisotropic source emission such an approach does not lead to satisfactory results.

Application of the method to eliminate multiple scattering features from the energy distribution is illustrated in Figs. 4(b)–6(b). The deconvolution formula Eq. (13) was applied to the model spectra in Figs. 4(a)–6(a) resulting in the true intrinsic spectrum. Subtracting this result from the model spectra yields the contribution from the background of inelastically scattered electrons, which is represented by the dotted lines in Figs. 4(a)–6(a). As a measure of the accuracy of the background subtrac-

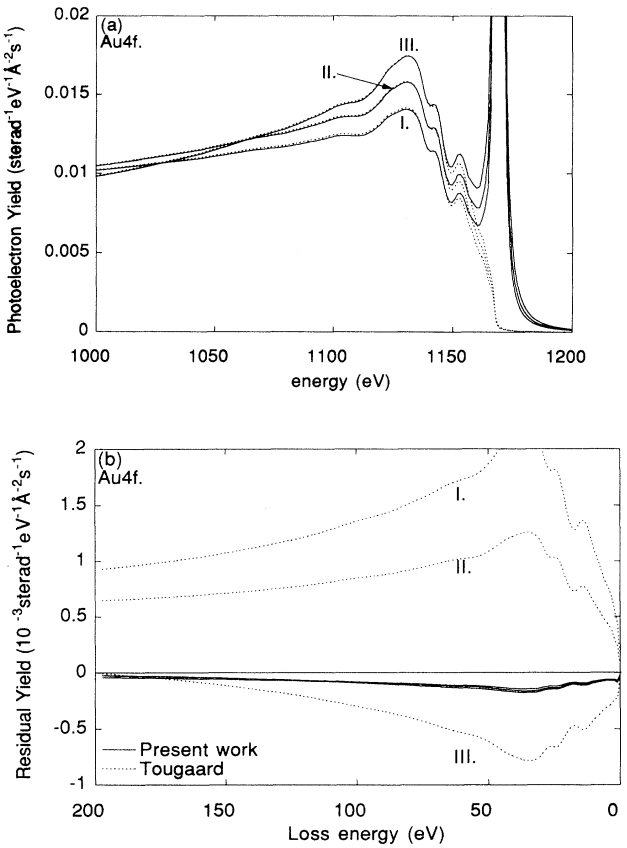

FIG. 5. Same as Fig. 4 for the Au $4f$ photoelectron line.

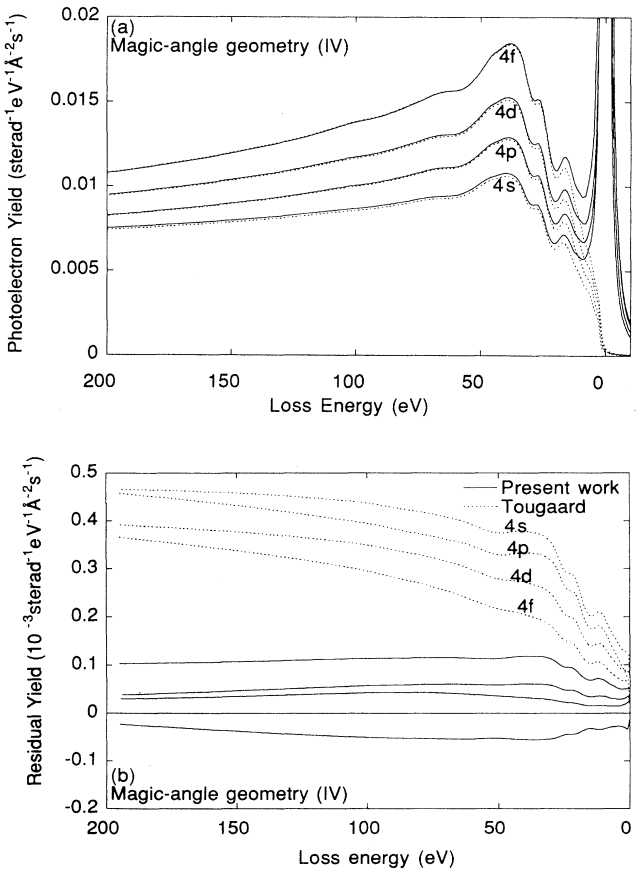

FIG. 6. Same as Fig. 4 for the magic angle geometries of all the studied subshell transitions.

tion we introduce the residual yield, i.e., the difference between the original intrinsic spectrum and the background corrected spectrum. This quantity is displayed in Figs. 4(b)–6(b) as solid lines and compared with the corresponding result using the algorithm by Tougaard (dotted lines). Note that the ordinate scale differs by a factor of 1000 from Figs. 4(a)–6(a).

In all cases the present method leads to background corrected spectra agreeing with the true model spectra within 2–3 % over the entire energy interval. These small discrepancies are entirely attributable to the minor deficiency of the transport approximation (cf. Fig. 2) as an assessment shows in which the MC results for the PED's were used in the deconvolution. This yields agreement to within a tenth of a percent over the entire energy interval.

The approach of Tougaard is seen to work reasonably well only for the (probably most important) case of the magic angle geometry [see Fig. 6(b)]. Even in that case, however, due to the significant underestimate in the background level of 5–10 % this procedure is slightly inferior to the present method, especially in terms of peak area quantification. As far as line-shape analysis is concerned, both methods can be said to be equivalent in such a geometry.

This is certainly not the case for the other selected geometries. After correction for multiple scattering with Tougaard's method, the background is seen to contain a considerable amount of structure for which obviously the DIIMFP and not the intrinsic spectrum is responsible [(Figs. 4(b) and 5(b)]. The background level is also seen to be over- or underestimated by up to 30%, depending on the geometry. These discrepancies are more serious for larger asymmetry parameters. Moreover, the differences between the corrected spectrum and the true spectrum are the largest for geometries in which the source angular distribution is low. This indicates that the neglect of the anisotropic source distribution in this approach generally leads to quite severe discrepancies in the angular and/or energy distribution (as was to be expected on the basis of Fig. 1) making application of this algorithm to XPS data for an arbitrary geometry rather questionable.

A few points are due to be discussed at this stage. The presented results show that the proposed theory accurately describes the photoelectron energy and/or angular distribution for noncrystalline solids in the quasielastic regime. The fact that the theory applies to random solids is not as severe a restriction as it may seem at first sight. Of course, in single crystals λ coherent scattering effects constitute the predominant features in the photoelectron angular distribution, as evidenced by many works on photoelectron diffraction. But the point is that the energy dissipation process of a signal electron leads to irreversible thermalization of the electron flux density and with increasing energy loss an increasing fraction of electrons belongs to the group of incoherently scattered electrons.[40] The incoherently propagating electrons obey a Boltzmann type transport equation, which is equivalent to the quantum kinetic equation in the limit of a completely disordered (random) solid. This implies that the inelastic background in a photoelectron spectrum can be expected to exhibit much less structure originating from the crystalline state of the solid than the (elastic) peak. This has in fact been observed in several studies of Auger and photoelectron diffraction. Egelhoff[41] reports that the inelastic background from a single crystal Ni(100) surface exhibits no observable enhancement in a direction where the peak areas are strongly increased by forward focusing. A detailed study of the angular distribution of photoelectron core level and plasmon peaks from the Al(001) surface led Osterwalder and co-workers[42] also to the conclusion that coherent effects are strongly suppressed in the inelastic tail of the spectrum. However, a small amount of structure due to the crystallinity of the solid was observed in the inelastic background in this case. These findings indicate that the present theory for the inelastic background in a random solid is also of relevance for the incoherent part (or inelastic tail) of energy spectra from crystalline solids.

As to the problem of energy ranges exceeding the quasielastic regime, there exists substantial evidence that this restriction may also be removed, or at least be relaxed. For instance, Tougaard[43] notes that reasonable background subtraction is obtained over an energy range of more than 1000 eV without any regard for the fact that this is almost always considerably larger than the quasielastic regime in XPS. A possible explanation for this fact is that the energy dependence of the yield is mainly determined by the transport mean free path, while the partial escape distributions only depend on the scattering parameter χ, which varies only very weakly with the energy. This suggests that the energy dependence for the yield beyond the quasielastic regime may to a first approximation be accounted for by considering the energy dependence of λ_{tr} in Eq. (3).

As a final point to be discussed, it is emphasized once more that the present background subtraction method can be applied in a straightforward manner to many problems in physics concerning removal of multiple scattering features from experimental data. This seems particularly promising for the extraction of the dielectric loss function from experimental reflection energy loss spectra (REELS). It has been recently shown[44] by analysis of experimental spectra and comparison with model calculations that the energy distribution in a REELS depends on the scattering geometry, owing to the fact that the path length distribution in the reflection geometry (where a well collimated electron beam is used to probe the surface) is strongly determined by the exact shape of the elastic scattering cross section. Note that this also follows directly from the generalized radiative field similarity principle. On the other hand, an accurate expression for the zero order reflection distribution was derived and compared with experimental data in Ref. 27. The mathematical structure of the terms entering this expression strongly resembles the one in Eq. (6). Therefore calculation of the partial reflection distributions is straightforward. In order to retrieve L_1 from the experimental spectrum instead of f, the Laplace transform of the DIIMFP can be expanded in terms of $\tilde{y} - 1$, leading to a deconvolution formula similar to Eq. (13). For an effective application to experimental data in the medium energy range, an accurate description of surface excita-

tions is mandatory, however. Discussion of this point is beyond the scope of the present paper and will be published elsewhere.

VI. SUMMARY

The influence of multiple elastic and inelastic scattering on photoelectron spectra from semi-infinite random solids has been studied. A theory accounting for the influence of the relevant phenomena on the line shape has been presented and compared with model calculations. From this comparison it may be concluded that the influence of anisotropic source emission in XPS can be adequately described in the framework of the transport approximation. The energy and angular distribution obtained for four subshell transitions in Au shows quite strong influences of the source anisotropy. Neglect of this effect in general can lead to rather misleading results of background subtraction procedures. For example, the only case where satisfactory results were found using Tougaard's method is the (of course very important) magic angle geometry. A background subtraction method has been developed which does not suffer from this drawback and yields quite perfect background removal in all studied cases. Moreover, the generality of the proposed method is encouraging in that it allows straightforward application to similar problems in other areas of physics.

APPENDIX: EXPLICIT EXPRESSION FOR THE PARTIAL ESCAPE DISTRIBUTIONS

The n-fold differentiation of Eq. (6) can be performed term by term using Cauchy's integral formula. For the third term this is trivial. The general procedure will be outlined in some detail for the first term.

Using the effective approximation of the Chandrasekhar H function presented in Ref. 7:

$$H(\mu,\omega)=\frac{1+\alpha}{1+\alpha\sqrt{1-\omega}}, \tag{A1}$$

where $\alpha=H(\mu,1)-1$, we may write the n-fold differentiation of the first term in the form

$$I_1(\mu)=\frac{1}{n!}\left[\frac{\partial^n}{\partial p^n}\frac{\omega^2(p)H(\mu,\omega(p))}{\sqrt{1-\omega(p)}}\right]\Bigg|_{p=0}$$
$$=\frac{1}{2\pi i}\oint_{C'}\frac{\omega^2(p)}{\sqrt{1-\omega(p)}}\frac{1+\alpha}{1+\alpha\sqrt{1-\omega(p)}}\frac{dp}{p^{n+1}}. \tag{A2}$$

In order to avoid dealing with the multivalued functions in the integrand, the substitution

$$s=\sqrt{1-\omega(p)}$$

is made. The integral then becomes

$$I_1(\mu)=\frac{\chi(1+\alpha)}{\pi i}\oint_C\left(\frac{s^2-1}{s^2(1+\chi)-1}\right)^{n+1}\frac{ds}{1+\alpha s}, \tag{A3}$$

where the contour C is a circle in the s plane around the point $(1+\chi)^{-1/2}$ on the real axis. After transformation of the integral as indicated in Fig. 7 we have to calculate the two integrals along the segments C_1 and C_R. Note that the latter integral does not vanish for $R\to\infty$. However, making the substitution $s=R\exp(i\phi)$ and taking the limit for large R, the contribution of C_R is immediately found to be given by

$$-\frac{\chi}{(\chi+1)^{n+1}}\frac{1+\alpha}{\alpha}. \tag{A4}$$

The integral along the imaginary axis may be evaluated directly by substituting $s=it$, yielding the sum of two integrals, one symmetric and one antisymmetric in t. The latter integral vanishes and a relatively simple real integral follows. Taking into account Eq. (A4), the final expression for the first term may be written as

$$I_1(\mu)=\frac{1}{n!}\left[\frac{\partial^n}{\partial p^n}\frac{\omega^2(p)H(\mu,\omega(p))}{\sqrt{1-\omega(p)}}\right]\Bigg|_{p=0}$$
$$=-\frac{\chi}{(\chi+1)^{n+1}}\frac{1+\alpha}{\alpha}$$
$$+\frac{\chi(1+\alpha)}{\pi}\int_{-\infty}^{\infty}\left(\frac{t^2+1}{t^2+1+\chi}\right)^{n+1}\frac{dt}{t^2+\alpha^2}. \tag{A5}$$

In an entirely analogous way one finds for the second term

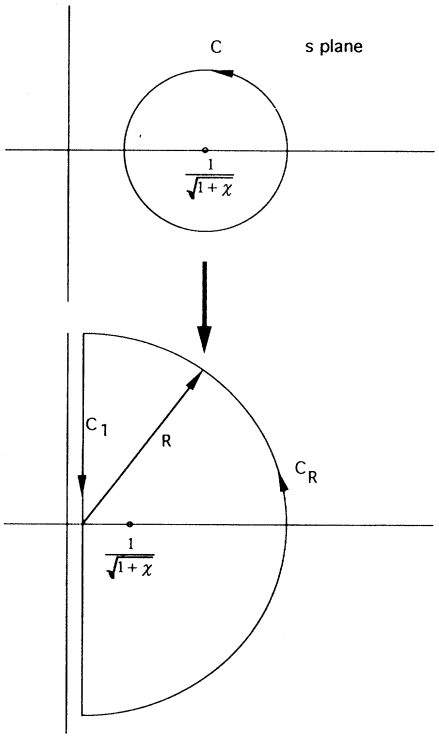

FIG. 7. Contours involved in the derivation of the explicit expression for the partial escape distribution (see text).

$$I_2(\mu,\mu_0)=\frac{1}{n!}\left[\frac{\partial^n}{\partial p^n}\omega^2(p)H(\mu,\omega(p))H(\mu_0,\omega(p))\right]\Bigg|_{p=0}$$
$$=-\frac{\chi}{(\chi+1)^{n+1}}\frac{1+\alpha}{\alpha}\frac{1+\beta}{\beta}+\frac{\chi(1+\alpha)(1+\beta)(\alpha+\beta)}{\pi}\int_{-\infty}^{\infty}\left(\frac{t^2+1}{t^2+1+\chi}\right)^{n+1}\frac{dt}{(t^2+\alpha^2)(t^2+\beta^2)}, \quad \text{(A6)}$$

where $\beta = H(\mu_0,1)-1$. The integrals in expressions (A5) and (A6) pose no problems for numerical evaluation, since they converge rapidly. The result for the third term may be found by direct differentiation or also by applying Cauchy's theorem and calculating the residue at $p=1+\chi$. This leads to

$$I_3=\frac{1}{n!}\left[\frac{\partial^n}{\partial p^n}\omega(p)\right]\Bigg|_{p=0}=\frac{\chi}{(\chi+1)^{n+1}}. \quad \text{(A7)}$$

Inserting expressions (A5), (A6), and (A7) into Eq. (6) we arrive at the final result for the partial escape distributions:

$$P_n(\vec{\Omega})=\frac{I_1(\mu)}{4\pi}-\frac{1}{4\pi}\int_0^1\frac{\mu_0 I_2(\mu,\mu_0)}{(\mu+\mu_0)}\bar{q}(\mu_0)d\mu_0+I_3 q(\vec{\Omega}). \quad \text{(A8)}$$

As a final remark it is noted that the function $H(\mu,1)$ may be approximated by the polynomial

$$H(\mu,1)-1=0.5073\mu^3-1.0016\mu^2+2.4102\mu,$$

which is usually sufficiently accurate and convenient for numerical calculations.

[1] *Practical Surface Analysis*, edited by D. Briggs and M.P. Seah (Wiley, Chichester, 1983).
[2] P. Staib and J. Kirschner, Appl. Phys. **3**, 421 (1974).
[3] D.A. Shirley, Phys. Rev. B **5**, 4709 (1972).
[4] H.H. Madden and J.E. Houston, J. Appl. Phys. **47**, 307 (1976).
[5] E.N. Sickafus, Surf. Sci. **100**, 529 (1980).
[6] M.F. Koenig and J.T. Grant, J. Electron Spectrosc. Relat. Phenom. **33**, 9 (1984).
[7] I.S. Tilinin and W.S.M. Werner, Surf. Sci. **290**, 119 (1993).
[8] W.S.M. Werner and I.S. Tilinin, Prog. Surf. Sci. **46**, 241 (1994).
[9] W.S.M. Werner and I.S. Tilinin, J. Appl. Phys. **70/71**, 29 (1993).
[10] I.S. Tilinin and W.S.M. Werner, Phys. Rev. B **46**, 13 739 (1992).
[11] V.V. Sobolev, *A Treatise on Radiative Transfer* (Van Nostrand, Princeton, NJ, 1963).
[12] S. Tougaard and P. Sigmund, Phys. Rev. B **25**, 4452 (1982).
[13] S. Tougaard, Phys. Rev. B **34**, 6779 (1986).
[14] S. Tougaard and I. Chorkendorff, Phys. Rev. B **35**, 6570 (1987).
[15] A.L. Tofterup, Surf. Sci. **167**, 70 (1986).
[16] V.M. Dwyer and J.A.D. Matthew, Surf. Sci. **193**, 549 (1988).
[17] A.L. Tofterup, Surf. Sci. **227**, 157 (1990).
[18] W.S.M. Werner, I.S. Tilinin, H. Beilschmid, and M. Hayek, Surf. Interface Anal. **21**, 537 (1994).
[19] V.M. Dwyer and J.A.D. Matthew, Surf. Sci. **152/153**, 884 (1985).
[20] O.A. Baschenko, G.V. Machavariani, and V.I. Nefedov, J. Electron Spectrosc. Relat. Phenom. **34**, 305 (1984).
[21] A. Jablonski and J. Zemek, Phys. Rev. B **48**, 4799 (1993).
[22] A. Jablonski and C.J. Powell, Phys. Rev. B **50**, 4739 (1994).
[23] K.M. Case and P.F. Zweifel, *Linear Transport Theory* (Addison-Wesley, Reading, MA, 1967).
[24] A. Jablonski, Surf. Interface Anal. **14**, 659 (1989).
[25] W.H. Gries and W.S.M. Werner, Surf. Interface Anal. **16**, 149 (1990).
[26] P. Cumpson, Surf. Interface Anal. **20**, 727 (1993).
[27] W.S.M. Werner, I.S. Tilinin, and M. Hayek, Phys. Rev. B **50**, 4819 (1994).
[28] S.L. Dudarev and M.J. Whelan, Surf. Sci. **311**, L687 (1994).
[29] S. Chandrasekhar, *Radiative Transfer* (Dover, New York, 1960).
[30] I.S. Tilinin and W.S.M. Werner, Mikrochim. Acta **114/115**, 485 (1994).
[31] S. Tanuma, C.J. Powell, and D.R. Penn, Surf. Interface Anal. **11**, 577 (1988).
[32] *Handbook of Optical Constants of Solids*, edited by E.D. Palik (Academic Press, New York, 1985).
[33] D.R. Penn, Phys. Rev. B **35**, 482 (1985).
[34] A.C. Yates, Comput. Phys. Commun. **2**, 175 (1971).
[35] R.A. Bonham and T.G. Strand, J. Chem. Phys. **39**, 2200 (1963).
[36] R.F. Reilman, A. Msezane, and S.T. Manson, J. Electron Spectrosc. Relat. Phenom. **8**, 289 (1976).
[37] I.M. Band, Yu.I. Kharitonov, and M.B. Trzhazkovskaya, At. Data Nucl. Data Tables **23**, 443 (1979).
[38] H. Ebel, M.F. Ebel, and A. Jablonski, J. Electron Spectrosc. Relat. Phenom. **35**, 155 (1985).
[39] S. Tougaard, Surf. Interface Anal. **11**, 453 (1988).
[40] U. Fano and J.A. Stephens, Phys. Rev. B **34**, 438 (1986).
[41] W. F. Egelhoff, Jr., Phys. Rev. Lett. **30**, 1052 (1984).
[42] J. Osterwalder, T. Greber, S. Hüffner, and L. Schlapbach, Phys. Rev. B **41**, 12 495 (1990).
[43] S. Tougaard, Surf. Sci. **216**, 343 (1989).
[44] W.S.M. Werner and M. Hayek, Surf. Interface Anal. **22**, 79 (1994).